Phase transition and spin-resolved transport in MoS_2 nanoribbons

A. Heshmati-Moulai,[1,*] H. Simchi,[1,2] M. Esmaeilzadeh,[1,†] and F. M. Peeters[3]
[1]*Department of Physics, Iran University of Science and Technology, Narmak, Tehran 16844, Iran*
[2]*Semicondutor Technology Center, Tehran 19575-199, Iran*
[3]*Departement Fysica, Universiteit Antwerpen, Groenenborgerlaan 171, 2020 Antwerpen, Belgium*
(Received 28 September 2016; revised manuscript received 1 December 2016; published 20 December 2016)

The electronic structure and transport properties of monolayer MoS_2 are studied using a tight-binding approach coupled with the nonequilibrium Green's function method. A zigzag nanoribbon of MoS_2 is conducting due to the intersection of the edge states with the Fermi level that is located within the bulk gap. We show that applying a transverse electric field results in the disappearance of this intersection and turns the material into a semiconductor. By increasing the electric field the band gap undergoes a two stage linear increase after which it decreases and ultimately closes. It is shown that in the presence of a uniform exchange field, this electric field tuning of the gap can be exploited to open low energy domains where only one of the spin states contributes to the electronic conductance. This introduces possibilities in designing spin filters for spintronic applications.

DOI: 10.1103/PhysRevB.94.235424

I. INTRODUCTION

The miniaturization process of semiconductor devices has followed two strategies called "more Moore" and "more than Moore." In the latter, one of the important trends is finding new semiconductor materials [1–3]. Materials with sizable band gap are key materials for manufacturing field effect transistors (FET) and optoelectronic devices (OPD). The discovery of graphene has motivated scientists and technologists to study graphene-related materials (GRM) for applications in the next generation of nanodevices. Therefore, with zero-gap graphene in retrospect, finding sizable GRM for manufacturing nano-FETs and nano-OPDs constitutes the core of research activities in the more than Moore strategy. Transition metal dichalcogenides are a class of GRM with the formula MX_2, where M is a transition metal element from group VI (such as Mo, W, and so on) and X is a chalcogen (S, Se, or Te). The monolayer MX_2 possesses a variety of polytypic structures such as 1H, 1T, and 1T′. The 1H-MX_2 in ABA stacking and 1T-MX_2 in ABC stacking have space groups $P\bar{6}m2$ and $P\bar{3}m1$, respectively [4,5]. The 1T′-MX_2 is a distorted 1T-MX_2 structure with respect to some M atoms. Bulk MoS_2 is a semiconductor with an intrinsic band gap of 1.2 eV [6]. The monolayer MoS_2 has a honeycomb lattice with potential applications in two-dimensional nanodevices [7,8]. The monolayer MoS_2 is a direct gap semiconductor with a band gap of 1.8 eV [7] and can be easily synthesized using scotch tape or lithium-based intercalation [8,9]. The mobility of monolayer MoS_2 can be at least 200 $cm^2\,V^{-1}\,s^{-1}$ at room temperature using hafnium oxide as a gate dielectric [8]. Recently, MoS_2 nanoribbons have been manufactured using an electrochemical method [10]. Since MoS_2 is a direct band gap semiconductor, it is suitable for optical manipulations and opens access to many optoelectronic applications [7,11,12]. In addition, both valley polarization and valley coherence can be achieved by optical pumping with circularly and linearly polarized light in MoS_2 [13,14]. The electronic band structure and transport properties of bulk monolayer MoS_2 have been investigated using first principles and tight-binding models [15–23]. Magnetic exchange field induced with the use of ferromagnetic substrates [24] or an external magnetic field [25,26] have been recently shown to be effective candidates for creating spin and valley polarized currents in monolayer MoS_2 sheets.

Studying the same effects on nanoribbons turns out to be more challenging due to the appearance of edge states for which simple two-band models lose their effectiveness. Using spin-polarized first principle density functional theory (DFT), Li *et al.* showed that zigzag (armchair) nanoribbons of MoS_2 show ferromagnetic (nonmagnetic) and metallic (semiconducting) behaviors [27]. It has also been shown that an armchair nanoribbon of MoS_2 could be metallic and exhibits a magnetic moment and, when passivated with hydrogen, becomes semiconducting [28]. Zigzag nanoribbons of MoS_2 are metallic and exhibit unusual magnetic properties regardless of passivation [28]. Using first-principle calculation, Yue *et al.* showed that the band gap of armchair MoS_2 nanoribbons can be significantly reduced and even be closed by applying a transverse field, whereas such a band gap modulation is absent under perpendicular field [29]. It has been shown that tensile strain in the zigzag direction of a single-layer MoS_2 zigzag nanoribbon produces a reversible modulation of the magnetic moments and exhibits an electronic phase transition [30]. This strain-induced modulation can be enhanced or suppressed further by applying an electric field [30].

The spin-dependent electronic structure and transport behavior of MoS_2 nanoribbons can be profoundly affected by the manipulation of the edges. This includes engineering various shapes of defects and passivating the edges with hydrogen or sulfur atoms [31]. Once these structural properties are imposed on these materials, they cannot be manipulated further during the actual use of the final device. To modify edge properties when in use, a better option would be to tamper with the electronic edge *states* rather than the edge *structure*. The idea is to use a gate that produces an electric field. The change induced in the material properties by applying an electric field could also involve topological phase transitions. One interesting example has been reported for the 1T′ structure of transition metal dichalcogenides, in which a vertical electric

*aheshmati@iust.ac.ir
†mahdi@iust.ac.ir

field can transform the quantum spin Hall phase into a trivial one by closing the gap in the material [32]. Such an electric field can also be used to enhance the spin-filtering properties that are initially induced by, e.g., defects [33] in graphene nanoribbons. This motivated us to investigate whether or not similar effects can be induced in MoS_2 nanoribbons which possess other interesting properties.

In this paper, we consider a monolayer of zigzag MoS_2 nanoribbon in the 1H structure. We show how tunable spin-resolved transport properties can be revealed in the presence of a transverse electric and a uniform exchange field. We find that by applying a transverse electric field, with a strength larger than a critical value, the inverted band gap disappears and the zigzag MoS_2 nanoribbon turns into a semiconductor. A uniform exchange field breaks time reversal symmetry but preserves band inversion. Consequently, the exchange field can be used to split the two spin states in a controllable manner. By applying simultaneously transverse electric and exchange fields, one can control the spin polarization, and perfect spin filtering in the nanoribbon becomes possible. The structure of our paper is as follows: In Sec. II, we describe the tight-binding model for MoS_2. The numerical results and discussions are presented in Sec. III, and a summary is given in Sec. IV.

II. BASIC FORMALISM

A. Tight-binding description of MoS_2

Xiao *et al.* [15] described the low-energy physics of monolayer MoS_2 around the K and K' points using a simple Dirac Hamiltonian. Cappelluti *et al.* [16] considered five orbitals ($4d_{x^2-y^2}$,$4d_{xy}$,$4d_{xz}$,$4d_{yz}$,$4d_{3z^2-r^2}$) for each molybdenum (Mo) atom and three orbitals ($3p_x$,$3p_y$,$3p_z$) for each sulfur (S) atom and introduced an 11-band Hamiltonian for single as well as multilayer MoS_2. By performing an appropriate unitary transformation which transforms the p orbitals of the top and bottom S atoms into their symmetric and antisymmetric combinations with respect to the z axis, one can write the Hamiltonian of monolayer MoS_2, around the energy gap, as [17]

$$H = \sum_{i,\mu\nu} \epsilon_{\mu,\nu} c^{\dagger}_{i,\mu} c_{i,\nu} + \sum_{ij,\mu\nu} [t_{ij,\mu\nu} c^{\dagger}_{i,\mu} c_{j,\nu} + \text{H.c.}], \quad (1)$$

where $c^{\dagger}_{i,\mu}(c_{i,\mu})$ creates (annihilates) an electron in the unit cell i in the atomic orbital labeled by $\mu = 1,\ldots,6$ belonging to the Hilbert space defined by the wave vector

$$\vec{\psi} = \left(d_{3z^2-r^2}, d_{x^2-y^2}, d_{xy}, p^S_x, p^S_y, p^A_z\right), \quad (2)$$

where the S and A superscripts of the p orbitals refer to symmetric and antisymmetric combinations $p^S_i = 1/\sqrt{2}(p^t_i + p^b_i)$ and $p^A_i = 1/\sqrt{2}(p^t_i - p^b_i)$, the index i runs over the spatial directions $i = x,y,z$, and the labels t and b refer to the top and bottom sulfur planes, respectively. Since all the hopping terms $t_{ij,\mu}$, and on-site energies, $\epsilon_{\mu,\nu}$, within a Slater-Koster scheme are given in Refs. [16,17], we will not repeat them here. The spin-orbit coupling (SOC) effect is included through the parameters $\langle d_{x^2-y^2}|H|d_{xy}\rangle = -i\lambda_M \hat{s}_z$ for the metal atom and $\langle p_x|H|p_y\rangle = -i\frac{\lambda_X}{2}\hat{s}_z$ for the chalcogen atoms where λ_M and λ_X stand for the SOC strength of metal and chalcogen atoms, respectively, and $\hat{s}_z = \pm$ indicates the z component of the spin degrees of freedom [17]. The spin-dependent conductance and spin polarization are studied using the tight-binding nonequilibrium Green's function method (TB-NEGF). The TB-NEGF method is explained in detail in our previous work [18].

B. Important notes about the Hamiltonian

Cappelluti *et al.* showed that at the K point, the minimum of the conduction band (MCB) is constructed from contributions of $4d_{3z^2-r^2}$ (0.82%) and $3p_x$,$3p_y$ (12%) and the other orbitals (6%) with even parity with respect to the $z \to -z$ inversion symmetry. They also showed that at the K point, the maximum of the valence band (MVB) is constructed from contributions of $4d_{x^2-y^2}$,$4d_{xy}$ (76%), $3p_x$,$3p_y$ (20%), and the other orbitals (4%) with even parity [16]. The energy difference between the MVB and MCB is 1.8 eV at the K point which is the band gap of monolayer MoS_2 [16]. It has been shown that the second maximum at the Γ point (just 42 meV below the real band edge at the K point) is composed of the $3p_z$ and $4d_{3z^2-r^2}$ orbitals [16]. By examining Eq. (2), we can conclude that the above-mentioned results are reproduced by the reduced Hilbert space $\vec{\psi}$ in which only the members with even parity with respect to the $z \to -z$ transformation are included.

III. NUMERICAL RESULTS AND DISCUSSION

The monolayer 1H-MoS_2 zigzag nanoribbon is schematically shown in Fig. 1. The length and width of the nanoribbon are taken along x and y directions, respectively, and the z direction is perpendicular to the Mo plane. In the following subsections, we consider two different cases, namely the case without including effects from the fields and the case in which the effects of one or both fields have been taken into account. This allows us to correctly analyze the effect of each term on the spin-resolved transport behavior of the nanoribbons.

A. Transport in the absence of any fields

Figure 2 shows the energy dispersion curve of the nanoribbon for the two spin states when the width of the nanoribbon is $W = 20$ Å. Because of time reversal symmetry the dispersion

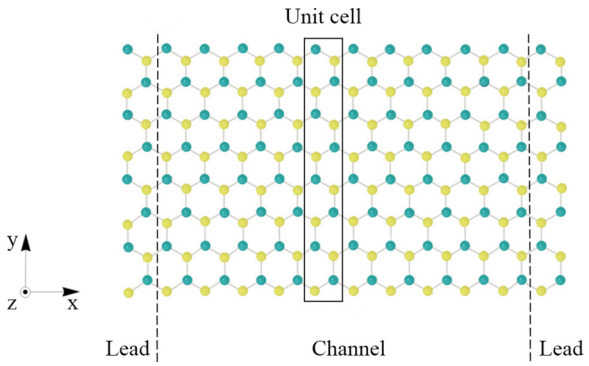

FIG. 1. A zigzag monolayer MoS_2 nanoribbon. Each unit cell includes 8 Mo atoms and 16 S atoms and the transport channel is composed of 240 atoms (i.e., we consider 10 unit cells along the nanoribbon). The channel is connected to semi-infinite monolayer nanoribbons of MoS_2 as left and right leads. Mo atoms and S atoms are shown in green and yellow color, respectively.

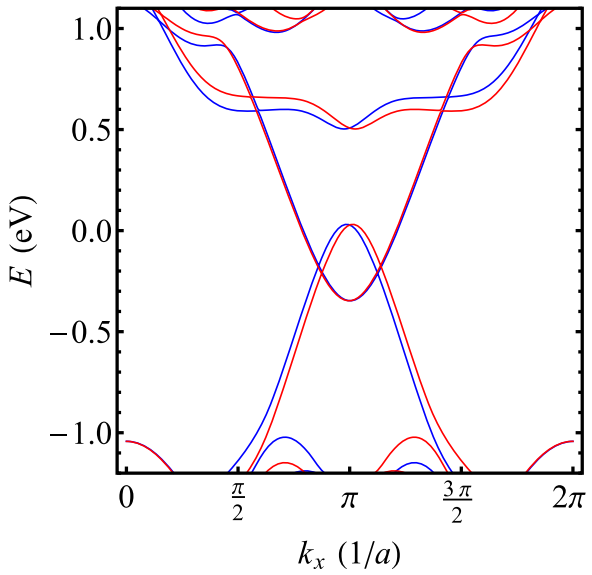

FIG. 2. Energy dispersion of a 8-ZMoS$_2$NR. The blue and red curves correspond to spin-up and spin-down states, respectively.

of spin-down states is the mirror image of this diagram with respect to the Γ point which is represented in this figure by $k_x = \pi/a$. As is apparent from the figure, the spectrum exhibits a band inversion for the edge states which intersect with each other at $k_x = 2.7/a$ and $k_x = 3.5/a$ where $a = 3.16$ Å is the Mo-Mo distance. No energy gap is seen in the intersection points, but the inverted gap (the energy difference between peak and valley at $k_x = \pi$ point) equals 0.4 eV.

Figure 3(a) shows the local density of states (LDOS) at the top Mo site (blue) and the bottom S site (red), and Fig. 3(b) shows the conductance versus the electron energy (E_e). An energy gap equal to 0.44 eV is seen in the LDOS for the top edge atoms, but we see finite conductance in Fig. 3(b) in this energy range. This means that the top edge has no contribution to the conductance in this energy interval. To better understand the nonzero conductance in the energy gap region of the LDOS, we plot the square of the wave function (SWF) [21], $|\psi_{i\mu}|^2$, which quantifies the relative contribution of the local orbitals to the density of states along the width of the nanoribbon. Figure 4 shows the SWF in this energy range at $k = 4/a$. It is apparent that the edge states in this energy range are composed almost exclusively of the orbital contributions from the bottom edge. This confirms the previous description of the behavior of these edge states [17–21]. The energy range where the stacking of states at the top edge exists (as can be seen in Fig. 2) starts from the top of the inverted gap region to the minimum of the next edge state. There is another interval below the inverted gap in which the exact opposite occurs, i.e., the top edge transport region. These two energy ranges manifest themselves as two minimum steps in the conductance [Fig. 3(b)].

B. The effect of external fields

1. Band gap opening by transverse electric field

Now we apply a transverse electric field via a gate voltage V_t to the nanoribbon in the y direction. This can be experimentally achieved by depositing two electrodes with the voltage $V_t/2$

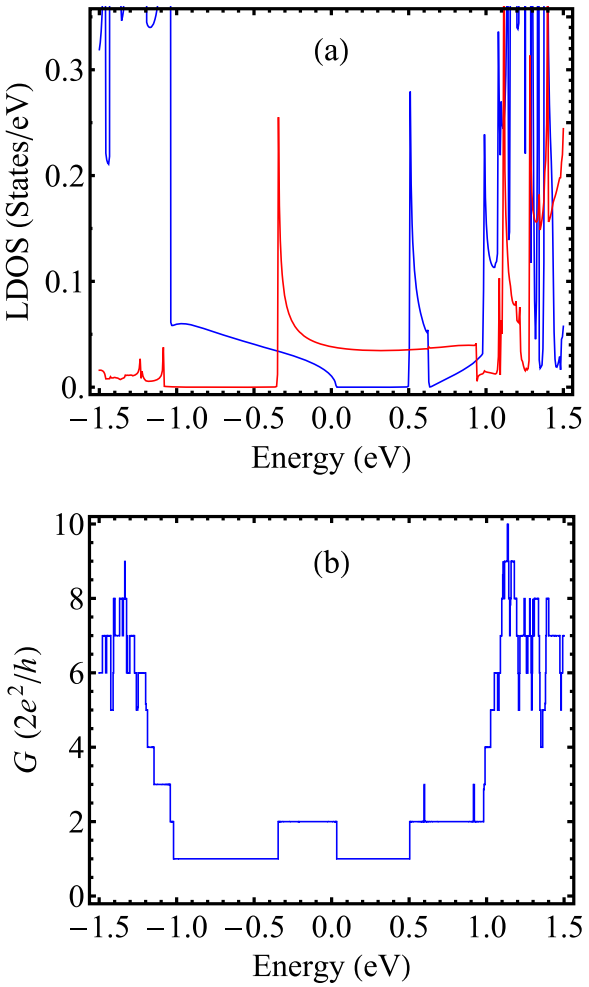

FIG. 3. (a) Local density of states at top Mo site (blue) and bottom S site (red) versus the electron energy for $N = 8$. (b) The conductance versus electron energy (without SOC and electric and exchange fields).

at $y = 0$ and $-V_t/2$ at $y = w$ to create the required uniform electric field across the MoS_2 nanoribbon as was previously proposed for graphene nanoribbons [34]. By increasing the electric field the inverted band gap in the intersection region begins to vanish. Then a regular energy band gap opens which linearly increases with the electric field. Figure 5(a) shows the band gap versus V_t. As the figure shows, there is a critical gate voltage V_c such that for voltages smaller than V_c the inverted gap is preserved for this nanoribbon width and consequently metallic properties are preserved. Changing the transverse electric field opens the gap linearly to a point at which it transforms into a plateau with a small positive slope where it builds up to a maximum. Then it decreases linearly until it closes again. After the condition $V_t > V_c$ is met, a gap opens at the $k_x = \pi/a$ point and the nanoribbon behaves as a semiconductor. This linear dependence of the band gap with the magnitude of the transverse electric field modulation has been reported recently for the 1T′ structural phase [32]. In that case the transition between semiconducting and metallic phase happens in an opposite way in which the intrinsic gap begins to vanish linearly when the transverse electric field is increased from zero.

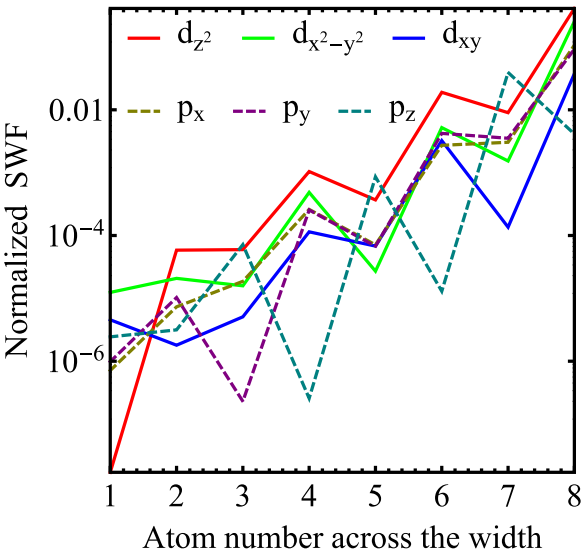

FIG. 4. Normalized square of the wave function, $|\psi_{i\mu}|^2$, of a nanoribbon with $N = 8$ versus the position across the width for an edge state above the inverted gap at $k_x = 4/a$ corresponding to an energy $E = 0.18$ eV. The relative contribution of the different orbitals is shown by solid lines for Mo orbitals and dashed lines for S orbitals.

Increasing the width of the nanoribbon has a small effect on the resulting band gap as shown in Fig. 5(b). For that reason all the results of this study are given for an 8-MoS_2NR. The maximum amount possible for the opened band gap is 0.52 eV as shown in Fig. 5(c). This maximum actually depends slightly on the nanoribbon width, nevertheless a value of 0.5 eV can be reached by an appropriate value of the gate voltage for any chosen width as can be inferred from the figure. Interestingly, this maximum is roughly of the same magnitude as the one for semiconducting armchair MoS_2 nanoribbons [35] in the absence of any field.

Although the TB model does not have the capability to describe the half metallicity as predicted by first principles calculations [36–38] in graphene, it has been successfully used to describe the band gap tuning by a transverse electric voltage in nanoribbons of graphene [34]. The main difference between graphene and MoS_2 is that ZGNR does not have band inversion properties, and increasing the electric field merely amounts to separating the partially flat bands around the Fermi energy in ZGNR. Thus graphene does not involve any interesting phase transition from a topological point of view.

2. *The effect of an exchange field*

If we introduce a ferromagnetic strip as a substrate, the magnetic proximity effect causes the two spin states in the entire Brillouin zone to move away from each other. This phenomenon can be taken into account by adding the term $\hat{s}_z M \sum_{i,\mu\nu} c^{\dagger}_{i,\mu} c_{i,\nu}$ in which M is the magnitude of the exchange energy [39]. This can be realized using a ferromagnetic insulator such as EuO or EuS for which the induced exchange energy ranges from 5 meV in graphene [40] to a giant magnitude of 0.2 eV in a transition metal dichalcogenide [41,42]. We will however investigate the gap opening for exchange energies in a slightly wider range (0.0 to 0.4 eV)

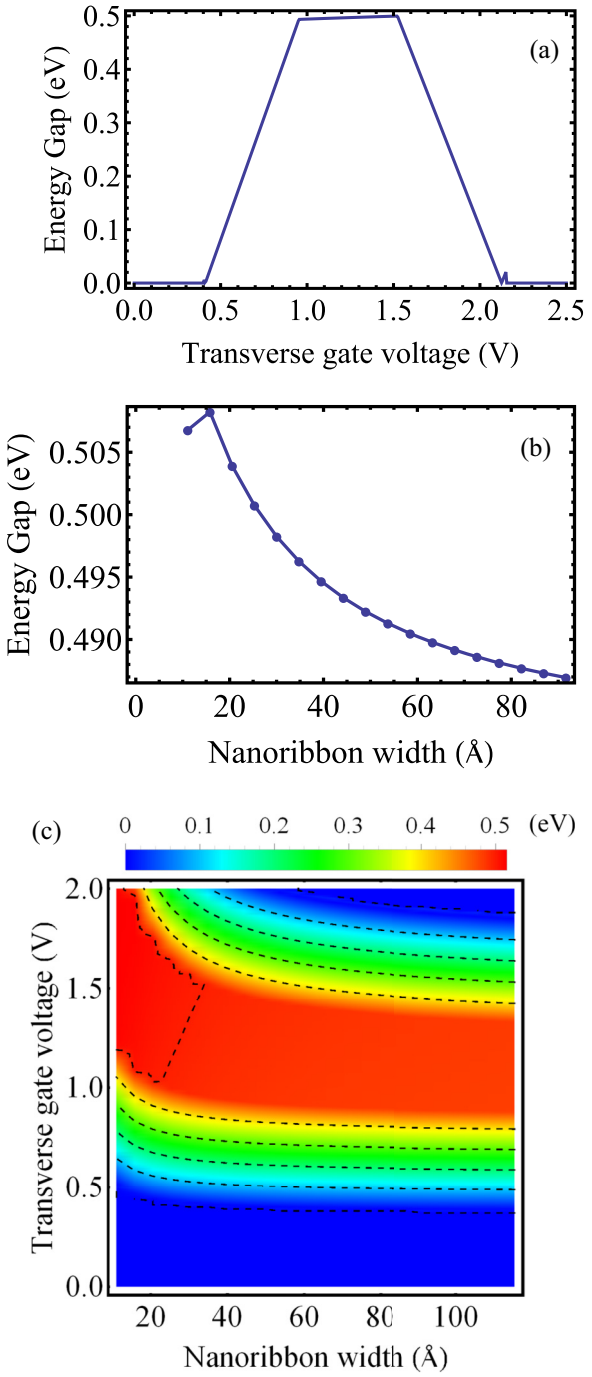

FIG. 5. A transverse electric voltage across the width of the nanoribbon is applied. (a) The band gap versus gate voltage for an 8-MoS_2NR. (b) Variation of the band gap with nanoribbon width. The value of the transverse field is in the plateau interval. (c) Contour plot of the band gap versus transverse electric voltage and width of the nanoribbon.

to be sure to include any possible experimental results in MoS_2. In contrast with the spin splitting induced by spin-orbit coupling, exchange splitting breaks the time reversal symmetry which is crucial for spin-polarizing electronic transport. The exchange field shifts the spin-up bands to higher or lower values depending on the sign of the exchange energy M, and the opposite occurs for the spin-down state. This result is

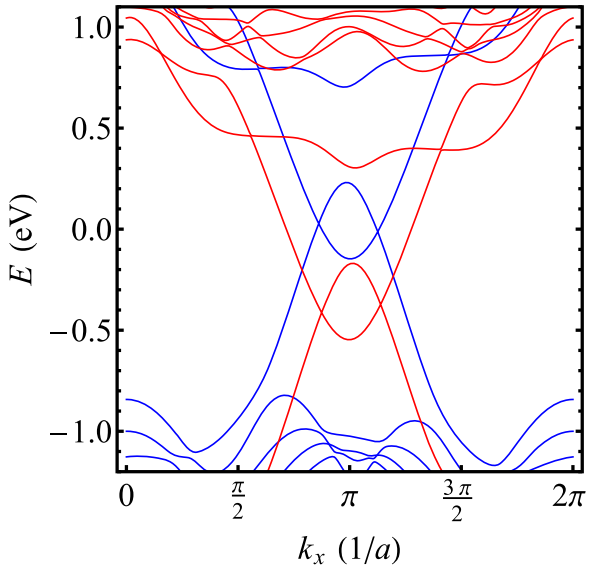

FIG. 6. Energy dispersion of a 8-ZMoS$_2$NR when a uniform exchange field with energy $M = 0.2$ eV is applied throughout the nanoribbon width. The spin-up bands are shown in blue and spin-down bands in red.

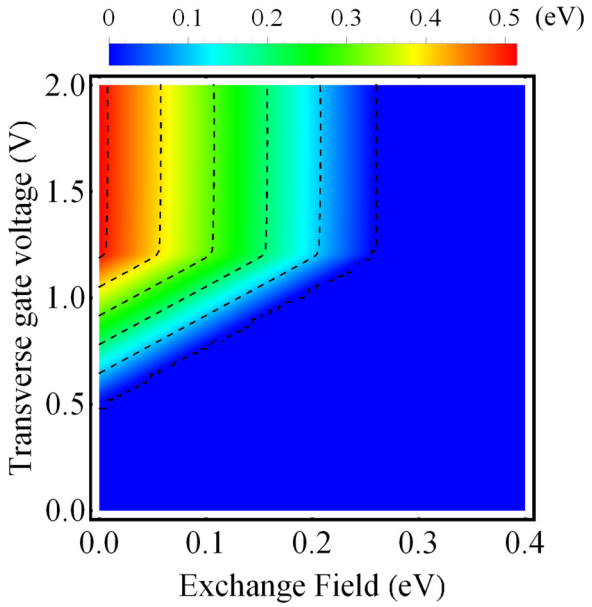

FIG. 7. Contour plot of the variation of the energy gap versus the electric and exchange fields for an 8-MoS$_2$NR. The gap can be opened to a maximum of about 0.5 eV.

depicted in Fig. 6 for a 8-ZMoS$_2$NR. Before applying the exchange field, the time reversal symmetry would transform the two spin states by $k \rightarrow -k$. This relation is destroyed as can be seen in the figure because the exchange interaction breaks the TRS. The energy spectrum will never exhibit a gap as a result of this type of field alone. As we will see in the next section adding an external electric field will cause the exchange field to be a gap tuning agent as well. Also any δE chosen in the energy range around the Fermi level always contains states of both spin types, and thus electronic transport is expected to be the result of both spin states. This will be changed in the following subsection where we turn on a transverse electric field.

3. *Perfect spin filtering*

The ultimate goal of spin filtering relies upon a time reversal symmetry breaking which splits the spin states in the energy spectrum as a necessary but not sufficient condition, as we accomplished in previous section. Now, we turn the transverse electric field on. The energy gap which was previously opened by applying the transverse electric field starts to disappear once we turn on the exchange field and will be closed completely when the exchange energy reaches a value of about 0.25 eV. This can be seen in Fig. 7 showing the variation of the band gap versus V_t and M when the width of the nanoribbon is equal to 20 Å. The mechanism of this band gap closing is in contrast with the previous one where only the electric field was able to tune it. In this case the energy gap in the spectrum of one of the spin states is filled by edge states which have the opposite spin state. An example can be seen in Fig. 8 showing the energy dispersion of a nanoribbon under the effect of an exchange field with exchange energy $M = 0.2$ eV and a transverse electric field corresponding to the potential $V_t = 0.85$ V. There is an energy region (-0.6 eV $< E < -0.2$ eV) with only spin-up states as well as a region filled exclusively with spin-down states (-0.2 eV $< E < 0.2$ eV) around the Fermi energy.

Now if we retain all of the parameters which were used to obtain Fig. 8 and increase the electric field slightly, the touching of spin-up and spin-down bands at -0.2 eV disappears and an energy gap opens. This could be inferred from Fig. 7 assuming we keep a constant exchange energy of 0.2 eV and increase the electric field. This way we can create a three-state switch with spin-up-passing/block-

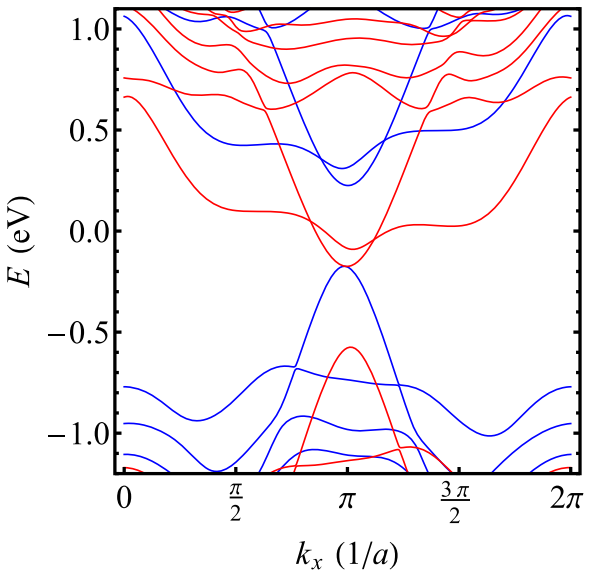

FIG. 8. Energy dispersion of an 8-ZMoS$_2$NR when an exchange field with exchange energy $M = 0.2$ eV and an electric potential $V_t = 0.85$ V are applied throughout the nanoribbon width. The blue curves are for the spin-up bands and the red curves are for the spin-down band.

both/spin-down-passing states depending on the electrochemical potential.

It is instructive to compare this electronic structure with the one of a graphene nanoribbon in the presence of a transverse electric field. It is well known that applying a transverse field to zigzag graphene nanoribbons leads to a half-metallic state [36–38]. In the half-metallic state, there exists an energy interval in which only one of the spin states contributes to the conductance. This means that for the other states there is an energy gap in the band structure. In other words, one of the spin states is filtered when we consider transport in that energy range while such a filtering won't occur for the other spin state. In our case, both spin states have their own band gaps in different energy intervals. Thus we have spin filtering for both spin states depending on the magnitude of the electrochemical potential. The energy gaps of the two spin states can be overlapping depending on the magnitude of the electric field. What is represented in Fig. 8 corresponds to the case for which the gaps are adjacent to each other.

This result can be taken advantage of for creating a spin-filtering device such that by tuning the energy of the charge carriers in this energy interval, we will be able to switch the type of the filter to be spin-up or spin-down. For this purpose we use the NEGF method to calculate the conductance of the nanoribbon with respect to the carrier energy. The results are depicted in Fig. 9(a) as a representative of a perfect spin filter. This effect is achievable for other values of fields the whole range of which is included in the density map of polarization for different values of the fields in Fig. 9(b). The dark red and dark blue patches distinguishable in Fig. 9(b) are regions in which the system becomes perfectly polarized for spin-down and spin-up states, respectively.

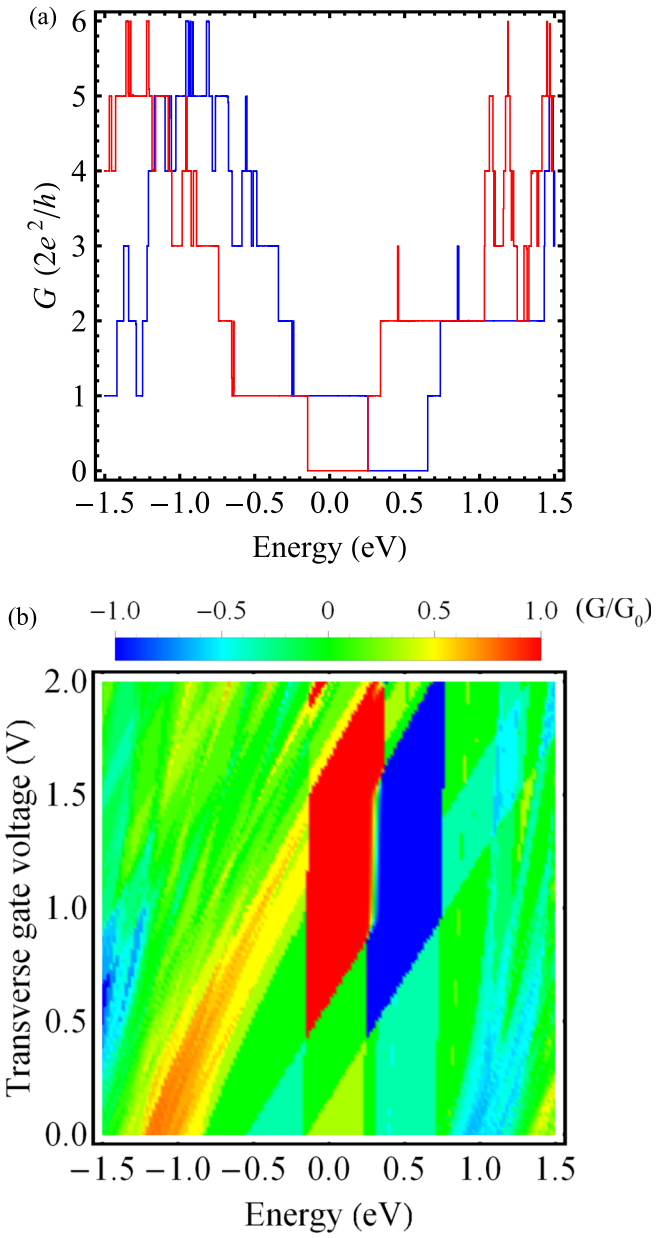

FIG. 9. Conductance and spin polarization of conductance in an 8-ZMoS$_2$NR. (a) Quantum conductance as a function of energy for the spin-up (blue curve) and spin-down (red curve) particles. (b) Cumulative effect of carrier energy and transverse electric field on the spin polarization of the conductance for an exchange energy of 0.2 eV. The dark red and dark blue spots correspond to perfect spin-up and spin-down filters, respectively.

4. Spin filtering in the presence of defects

While pristine nanoribbons of MoS_2 have been recently realized in laboratory [43,44], scalable production of this material without defects is still a technological challenge. Therefore it is important to examine how deviations from pristine nanoribbons can affect the functionality of the device. These defects usually occur as vacancies at the edges of nanoribbons. Figure 10 shows the change in conductance for the same system as the one depicted in Fig. 9(a) but with

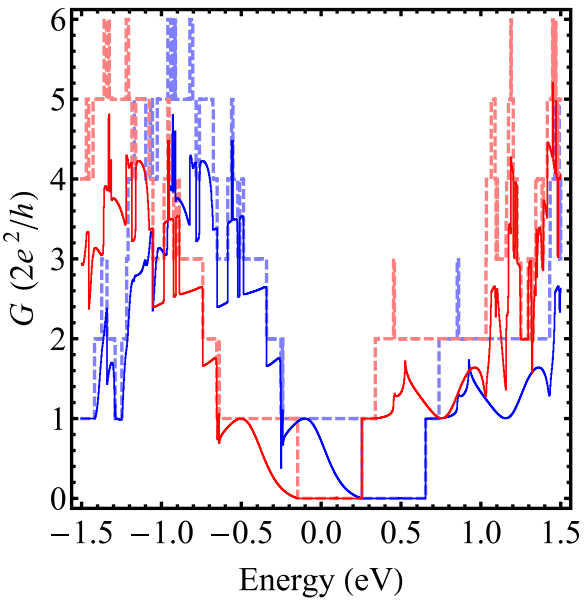

FIG. 10. Conductance of an 8-ZMoS$_2$NR with an isolated Mo defect at the top edge. The curves of Fig. 9 are repeated as dashed curves to make the deviations from the perfect system more evident. Blue and red curves represent the conductance for spin-up and spin-down states, respectively.

an isolated Mo vacancy at the top edge. The conductance of a perfect nanoribbon is shown by the dashed curve to make the comparison easier. The results reveal that in the energy range where the system filters the spin-up carriers (around $E = 0.0$ eV), the conductance of spin-down states is still zero and perfect filtering remains intact. The same happens for the spin-down filtering (around $E = 0.5$ eV). Thus the vacancies at the edges have no effect whatsoever on the functionality of the device. Our calculations show that the same is true for a sulfur vacancy at the bottom edge. In the energy range where perfect spin filtering occurs the defective system shows a lower conductance (solid curves) as compared to the perfect one (dashed curves) because of the reflections from the defect site, but for both spin states there are intervals in which the magnitude of the conductance reaches more than half of the previous one.

IV. SUMMARY AND CONCLUSION

The spin dependent transport properties in a monolayer MoS_2 zigzag nanoribbon were studied using the tight-binding NEGF method. We showed that applying a transverse electric field can turn the metallic zigzag MoS_2 nanoribbon into a semiconductor. This will destroy the intrinsic band inversion characteristics, and the opened energy gap can be linearly tuned up to a maximum of 0.52 eV by using a gate voltage. This maximum value corresponds roughly to that for armchair nanoribbons. Also the linear dependence of the band gap increase/decrease as a function of the transverse field parallels previously reported results for 1T′ structure which were based on a first principles approach. However, the here-found phase transition in the 1H structure occurs in the opposite direction, i.e., metal to semiconductor rather than semiconductor to metal.

When combined with the effect of an exchange field this property could be used to perfectly filter any chosen spin state. The results can help to open possibilities for designing spin filters and switches to be utilized in spintronic applications. On the other hand, the range of achievable direct energy gap between zero and 0.5 eV using just an electric field will boost the prospects of MoS_2 for optical applications. Because the opened band gap varies slowly with respect to the width of the nanoribbon, the band gap magnitude of 0.5 eV is achievable for virtually all nanoribbon widths, while for nanoribbons narrower than 30 Å the maximum is slightly larger than 0.5 eV. Calculations based on this model show that the perfect spin filtering is robust against isolated defects at the edges for both spin types.

ACKNOWLEDGMENT

We would like to thank K. Shakouri for helpful comments and discussion.

[1] G. E. Moore, Electronics **38**, 114 (1965).
[2] G. E. Moore, in *International Electron Devices Meeting* (IEEE, 1975), Vol. 21, pp. 11–13.
[3] W. Arden, M. Brillouet, P. Cogez, M. Graef, B. Huizing, and R. Mahnkopf, *"More-than-Moore" White Paper*, Tech. Rep. (ITRS, 2010).
[4] A. Molina-Sánchez and L. Wirtz, Phys. Rev. B **84**, 155413 (2011).
[5] S.-i. Nohara, H. Namatame, H. Matsubara, M. Fujisawa, M. Naitou, S. Tanaka, H. Negishi, M. Inoue, H. Sakamoto, A. Misu, and S. Suga, J. Phys. Soc. Jpn. **60**, 3882 (1991).
[6] K. K. Kam and B. A. Parkinson, J. Phys. Chem. **86**, 463 (1982).
[7] K. F. Mak, C. Lee, J. Hone, J. Shan, and T. F. Heinz, Phys. Rev. Lett. **105**, 136805 (2010).
[8] B. Radisavljevic, A. Radenovic, J. Brivio, V. Giacometti, and A. Kis, Nat. Nanotechnol. **6**, 147 (2011).
[9] A. Schumacher, L. Scandella, N. Kruse, and R. Prins, Surf. Sci. Lett. **289**, L595 (1993).
[10] Q. Li, J. T. Newberg, E. C. Walter, J. C. Hemminger, and R. M. Penner, Nano Lett. **4**, 277 (2004).
[11] A. Splendiani, L. Sun, Y. Zhang, T. Li, J. Kim, C. Y. Chim, G. Galli, and F. Wang, Nano Lett. **10**, 1271 (2010).
[12] A. Kuc, N. Zibouche, and T. Heine, Phys. Rev. B **83**, 245213 (2011).
[13] Z. Li and J. P. Carbotte, Phys. Rev. B **86**, 205425 (2012).
[14] T. Cao, G. Wang, W. Han, H. Ye, C. Zhu, J. Shi, Q. Niu, P. Tan, E. Wang, B. Liu, and J. Feng, Nat. Commun. **3**, 887 (2012).
[15] D. Xiao, G.-B. Liu, W. Feng, X. Xu, and W. Yao, Phys. Rev. Lett. **108**, 196802 (2012).
[16] E. Cappelluti, R. Roldán, J. A. Silva-Guillén, P. Ordejón, and F. Guinea, Phys. Rev. B **88**, 075409 (2013).
[17] H. Rostami, R. Roldán, E. Cappelluti, R. Asgari, and F. Guinea, Phys. Rev. B **92**, 195402 (2015).
[18] K. Shakouri, H. Simchi, M. Esmaeilzadeh, H. Mazidabadi, and F. M. Peeters, Phys. Rev. B **92**, 035413 (2015).
[19] H. Rostami and R. Asgari, Phys. Rev. B **89**, 115413 (2014).
[20] H. Rostami and R. Asgari, Phys. Rev. B **91**, 075433 (2015).
[21] H. Rostami, R. Asgari, and F. Guinea, J. Phys.: Condens. Matter **28**, 495001 (2016).
[22] T. Wolfram and Ş. Ellialtıoğlu, *Applications of Group Theory to Atoms, Molecules, and Solids* (Cambridge University Press, New York, 2014).
[23] O. Vafek and A. Vishwanath, Annu. Rev. Condens. Matter Phys. **5**, 83 (2014).
[24] P. M. Krstajić, P. Vasilopoulos, and M. Tahir, Physica E **75**, 317 (2016).
[25] M. Tahir, P. Vasilopoulos, and F. M. Peeters, Phys. Rev. B **93**, 035406 (2016).
[26] P. M. Krstajić, P. Vasilopoulos, and M. Tahir, Phys. Rev. B **94**, 085413 (2016).
[27] Y. Li, Z. Zhou, S. Zhang, and Z. Chen, J. Am. Chem. Soc. **130**, 16739 (2008).
[28] A. R. Botello-Méndez, F. López-Urías, M. Terrones, and H. Terrones, Nanotechnology **20**, 325703 (2009).
[29] Q. Yue, S. Chang, J. Kang, X. Zhang, Z. Shao, S. Qin, and J. Li, J. Phys.: Condens. Matter **24**, 335501 (2012).
[30] L. Kou, C. Tang, Y. Zhang, T. Heine, C. Chen, and T. Frauenheim, J. Phys. Chem. Lett. **3**, 2934 (2012).

[31] X.-M. Li, M.-Q. Long, L.-L. Cui, J. Xiao, X.-J. Zhang, D. Zhang, and H. Xu, Phys. Lett. A **378**, 2701 (2014).
[32] X. Qian, J. Liu, L. Fu, and J. Li, Science **346**, 1344 (2014).
[33] G. P. Tang, J. C. Zhou, Z. H. Zhang, X. Q. Deng, and Z. Q. Fan, Carbon **60**, 94 (2013).
[34] W. Apel, G. Pal, and L. Schweitzer, Phys. Rev. B **83**, 125431 (2011).
[35] H. Pan and Y.-W. Zhang, J. Mater. Chem. **22**, 7280 (2012).
[36] Y.-W. Son, M. L. Cohen, and S. G. Louie, Nature (London) **444**, 347 (2006).
[37] E.-J. Kan, Z. Li, J. Yang, and J. G. Hou, Appl. Phys. Lett. **91**, 243116 (2007).
[38] Y. Guo, W. Guo, and C. Chen, J. Phys. Chem. C **114**, 13098 (2010).
[39] Z. Qiao, S. A. Yang, W. Feng, W.-K. Tse, J. Ding, Y. Yao, J. Wang, and Q. Niu, Phys. Rev. B **82**, 161414 (2010).
[40] H. Haugen, D. Huertas-Hernando, and A. Brataas, Phys. Rev. B **77**, 115406 (2008).
[41] J. Qi, X. Li, Q. Niu, and J. Feng, Phys. Rev. B **92**, 121403 (2015).
[42] Q. Zhang, S. A. Yang, W. Mi, Y. Cheng, and U. Schwingenschlögl, Adv. Mater. **28**, 959 (2016).
[43] Z. Wang, H. Li, Z. Liu, Z. Shi, J. Lu, K. Suenaga, S.-K. Joung, T. Okazaki, Z. Gu, J. Zhou, Z. Gao, G. Li, S. Sanvito, E. Wang, and S. Iijima, J. Am. Chem. Soc. **132**, 13840 (2010).
[44] D. S. Fox, Y. Zhou, P. Maguire, A. O'Neill, C. Ó'Coileáin, R. Gatensby, A. M. Glushenkov, T. Tao, G. S. Duesberg, I. V. Shvets, M. Abid, M. Abid, H.-C. Wu, Y. Chen, J. N. Coleman, J. F. Donegan, and H. Zhang, Nano Lett. **15**, 5307 (2015).